The Quench-Action method in integrable spin chains: A Monte Carlo approach

Authors

Abstract.
fdasfa

1. Introduction

We show that it is possible to numerically simulate the Quench Action approach combining Monte Carlo methods and Bethe ansatz techniques.
We focus on the situation in which the pre-quench initial state is the Neel state or the Majumdar-Ghosh state.
We investigate the importance of the zero-momentum strings in the Quench Action.
Without zero-momentum strings the overlap saturation rules are not valid, i.e., in finite size systems the vast majority of the eigenstates contain zero momentum strings.
The details on the eigenstates counting depend on the pre-quench initial state.
However, we show that one can restrict to the set of non-zero momentum strings. The fact that one neglects zero-momentum strings gives rise only to scaling corrections.
We also investigate the validity of the Bethe-Takahashi approximation for the calculation of the overlap.
In the thermodynamic limit it is natural to assume that the steady-state expectation values are obtained using the so-called diagonal ensemble, which is defined as

$$\langle \mathcal{O} \rangle = \sum_{\alpha} |\langle \Psi_0 | \alpha \rangle|^2 \langle \alpha | \mathcal{O} | \alpha \rangle. \tag{1}$$

2. Bethe ansatz solution of the Heisenberg (XXX) spin chain

Here we review some Bethe ansatz results for the spin-$\frac{1}{2}$ Heisenberg (XXX) chain. Specifically, in section 2.1 we introduce the model. Its eigenstates (Bethe states) and the Bethe equations are discussed in section 2.2. Section 2.3 focuses on the string hypothesis and the so-called Bethe-Gaudin-Takahashi (BGT) equations. The form of the BGT equations in the thermodynamic limit is discussed in section 2.4. Finally, in section 2.5 we provide some exact formulas for the local conserved charges of the model.

2.1. The spin-$\frac{1}{2}$ Heisenberg chain

The spin-$\frac{1}{2}$ isotropic Heisenberg chain (XXX chain) with L sites is defined by the Hamiltonian

$$\mathcal{H} \equiv J \sum_{i=1}^{L} \left[\frac{1}{2} (S_i^+ S_{i+1}^- + S_i^- S_{i+1}^+) + S_i^z S_{i+1}^z \right], \tag{2}$$

where $S_i^{\pm} \equiv (\sigma_i^x \pm i\sigma_i^y)/2$ are spin operators acting on the site i, $S_i^z \equiv \sigma_i^z/2$, and $\sigma_i^{x,y,z}$ the Pauli matrices. We fix $J = 1$ and use periodic boundary conditions, identifying sites $L+1$ and 1. The total magnetization $S_T^z \equiv \sum_i S_i^z = L/2 - M$, with M number of down spins (particles), commutes with (2), and it is here used to label its eigenstates.

2.2. Bethe equations and wavefunctions

In the Bethe ansatz framework [3, 4] the generic eigenstate of (2) (Bethe state) in the sector with M particles can be written as

$$|\Psi_M\rangle = \sum_{1\leq x_1<x_2<\ldots<x_M\leq L} A_M(x_1,x_2,\ldots,x_M)|x_1,x_2,\ldots,x_M\rangle, \tag{3}$$

where the sum is over the positions $\{x_i\}_{i=1}^M$ of the particles, and $A_M(x_1,x_2,\ldots,x_M)$ is the eigenstate amplitude corresponding to the particles being at positions $x_1,x_2,\ldots,x_M$. Here $A_M(x_1,x_2,\ldots,x_M)$ is given as

$$A_M(x_1,x_2,\ldots,x_M) \equiv \sum_{\sigma\in S_M} \exp\Big[i\sum_{j=1}^M k_{\sigma_j}x_j + i\sum_{i<j}\theta_{\sigma_i,\sigma_j}\Big], \tag{4}$$

where the outermost summation is over the permutations S_M of the so-called quasi-momenta $\{k_\alpha\}_{\alpha=1}^M$. The two-particle scattering phases $\theta_{\alpha,\beta}$ are defined as

$$\theta_{\alpha,\beta} \equiv \frac{1}{2i}\log\Big[-\frac{e^{ik_\alpha+ik_\beta}-2e^{ik_\alpha}+1}{e^{ik_\alpha+ik_\beta}-2e^{ik_\beta}+1}\Big]. \tag{5}$$

The eigenenergy associated to the eigenstate (3) is

$$E = \sum_{\alpha=1}^M(\cos(k_\alpha)-1). \tag{6}$$

The quasi-momenta k_α are obtained by solving the so-called Bethe equations [3]

$$e^{ik_\alpha L} = \prod_{\beta\neq\alpha}^M\Big[-\frac{1-2e^{ik_\alpha}-e^{ik_\alpha+ik_\beta}}{1-2e^{ik_\beta}-e^{ik_\alpha+ik_\beta}}\Big]. \tag{7}$$

It is useful to introduce the rapidities $\{\lambda_\alpha\}_{\alpha=1}^M$ as

$$k_\alpha = \pi - 2\arctan(\lambda_\alpha) \mod 2\pi. \tag{8}$$

Taking the logarithm on both sides in (7), and using (8), one obtains the Bethe equations in logarithmic form as

$$\arctan(\lambda_\alpha) = \frac{\pi}{L}J_\alpha + \frac{1}{L}\sum_{\beta\neq\alpha}\arctan\Big(\frac{\lambda_\alpha-\lambda_\beta}{2}\Big), \tag{9}$$

where $-L/2 < J_\alpha \leq L/2$ are the so-called Bethe quantum numbers. The J_α are half-integers and integers for $L-M$ even and odd, respectively.

Finally, one should remark that M-particle eigenstates corresponding to *finite* rapidities are eigenstates with maximum allowed magnetization (highest-weight eigenstates) $S^z_T = L/2-M = S_T$, with S_T the total spin. Due to the $SU(2)$ invariance of (2), all the states in the same S_T multiplet and different $-S_T \leq S^z_T \leq S_T$ are eigenstates of the XXX chain with the same energy eigenvalue. These eigenstates (descendants) are obtained by multiple applications of the total-spin lowering operator $S^-_T \equiv \sum_i S^-_i$ on the highest-weight eigenstates. In the Bethe ansatz framework the rapidities of a generic M-particle descendant eigenstate with $S^T_T = L/2-M'$, with $M'<M$, are obtained by supplementing the M rapidities of the highest-weight state with $M'-M$ infinite rapidities. We anticipate that descendant eigenstates have non-zero overlap with the zero-momentum Néel state (cf. section 3).

2.3. String hypothesis & the Bethe-Gaudin-Takahashi (BGT) equations

In the thermodynamic limit $L \to \infty$ the solutions of the Bethe equations (7) form particular "string" patterns in the complex plane, (string hypothesis) [3, 4]. Specifically, the rapidities forming a "string" of length $1 \leq n \leq M$ (that we defined here as n-string) can be parametrized as

$$\lambda_{n;\gamma}^{j} = \lambda_{n;\gamma} - i(n-1-2j) + i\delta_{n;\gamma}^{j}, \qquad j = 0, 1, \ldots, n-1, \tag{10}$$

with $\lambda_{n;\gamma}$ being the real part of the string (string center), γ labelling strings with different centers, and j labelling the different components of the string. In Eq. (10) $\delta_{n;\gamma}^{j}$ are the string deviations, which typically, i.e., for most of the chain eigenstates, vanish exponentially with L in the thermodynamic limit. Note that real rapidities correspond to strings of unit length (1-strings), i.e., $n = 1$ in Eq. (10).
The string centers $\lambda_{n;\gamma}$ are obtained by solving the so-called Bethe-Gaudin-Takahashi equations

$$2L\theta_n(\lambda_{n;\gamma}) = 2\pi I_{n;\gamma} + \sum_{(m,\beta)\neq(n,\gamma)} \Theta_{m,n}(\lambda_{n;\gamma} - \lambda_{m;\beta}). \tag{11}$$

The generalized scattering phases $\Theta_{m,n}$ read

$$\Theta_{m,n}(x) \equiv \begin{cases} \theta_{|n-m|}(x) + \sum_{r=1}^{(n+m-|n-m|-1)/2} 2\theta_{|n-m|+2r}(x) + \theta_{n+m}(x) & \text{if} \quad n \neq m \\ \sum_{r=1}^{n-1} 2\theta_{2r}(x) + \theta_{2n}(x) & \text{if} \quad n = m \end{cases}$$

with $\theta_\alpha(x) \equiv 2\arctan(x/\alpha)$. Here $I_{n;\gamma}$ are the Bethe-Takahashi quantum numbers associated with $\lambda_{n;\gamma}$. The solutions of (11), and the Bethe states thereof, are naturally classified according to their "string content" $\mathcal{S} \equiv \{s_n\}_{n=1}^{M}$, with s_n the number of n-strings. Clearly, the constraint $\sum_{n=1}^{M} n s_n = M$ has to be satisfied. It can be shown that the BGT quantum numbers $I_{n;\gamma}$ associated with the n-strings are integers and half-integers for $L - s_n$ odd and even, respectively. An upper bound for the BGT quantum numbers can be derived as [4]

$$|I_{n;\gamma}| \leq I_n^{(MAX)} \equiv \frac{1}{2}(L - 1 - \sum_{m=1}^{M} t_{m,n} s_m), \tag{12}$$

where $t_{m,n} \equiv 2\min(n,m) - \delta_{m,n}$. Using the string hypothesis Bethe states energy eigenvalue (6) becomes

$$E = -\sum_{n,\gamma} \frac{2n}{\lambda_{n;\gamma}^2 + n^2}. \tag{13}$$

2.4. Thermodynamic limit

In the thermodynamic limit $L \to \infty$ at fixed finite particle density M/L the solutions of the BGT equations (11) become dense. One then defines the BGT root distributions for the n-strings as $\boldsymbol{\rho} \equiv \{\rho_n(\lambda)\}_{n=1}^{\infty}$, with $\rho_n(\lambda) \equiv \lim_{L\to\infty}[\lambda_{n;\gamma+1} - \lambda_{n;\gamma}]^{-1}$. Thus the

BGT equations (11) become an infinite set of coupled non-linear integral equations for the $\rho_n(\lambda)$ as

$$a_n(\lambda) = \rho_n(\lambda) + \rho_n^h(\lambda) + \sum_m (T_{n,m} * \rho_m)(\lambda), \tag{14}$$

where ρ_n^h are the hole-distributions, and the functions $a_n(\lambda)$ are defined as

$$a_n(x) \equiv \frac{1}{\pi} \frac{n}{x^2 + n^2}. \tag{15}$$

In (14) $T_{n,m} * \rho_m$ denotes the convolution

$$(T_{n,m} * \rho_m)(\lambda) \equiv \int_{-\infty}^{+\infty} T_{n,m}(\lambda - \lambda')\rho_m(\lambda'), \tag{16}$$

with the matrix $T_{n,m}(x) \equiv \Theta'(x)$ being dfined as

$$T_{m,n}(x) \equiv \begin{cases} a_{|n-m|}(x) + \sum_{r=1}^{(n+m-|n-m|-1)/2} 2a_{|n-m|+2r}(x) + a_{n+m}(x) & \text{if} \quad n \neq m \\ \sum_{r=1}^{n-1} 2a_{2r}(x) + a_{2n}(x) & \text{if} \quad n = m \end{cases}$$

2.5. The conserved charges

The XXX chain exhibits an extensive number of mutually commuting local conserved charges Q_n, with $n \in \mathbb{N}$, i.e.,

$$[Q_n, \mathcal{H}] = 0 \quad \forall n \quad \text{and} \quad [Q_n, Q_m] = 0 \quad \forall n, m. \tag{17}$$

The eigenvalues q_n of the conserved charges over the Bethe eigenstates (cf. (3)) are given as

$$q_{n+1} \equiv \frac{i}{(n-1)!} \frac{d^n}{dy^n} \log \tau(y) \Big|_{y=i}, \tag{18}$$

where y is a spectral parameter and $\tau(y)$ is the Bethe state eigenvalue of the so-called transfer matrix in the Algebraic Bethe Ansatz framework [5]. The analytic expression for $\tau(y)$ in terms of the solutions $\{\lambda_\alpha\}_{\alpha=1}^M$ of the Bethe equations (7) is given as

$$\tau(y) \equiv \left(\frac{y+i}{2}\right)^L \prod_\alpha \frac{y - \lambda_\alpha - 2i}{y - \lambda_\alpha} + \left(\frac{y-i}{2}\right)^L \prod_\alpha \frac{y - \lambda_\alpha + 2i}{y - \lambda_\alpha}. \tag{19}$$

Interestingly, from (18) one has that the second term in (19) does not contribute to q_n, at least for $n \leq L-2$. For a generic Bethe state q_n is obtained by summing independently the contributions of the BGT roots as

$$q_n = \sum_{k,\gamma} g_{n,k}(\lambda_{k;\gamma}). \tag{20}$$

Using the string hypothesis (10), and (18), (19), one obtains the the first few functions $g_{n,k}$ in terms of the solutions of the BGT equations as

$$\begin{aligned} g_{3,k} &= -\frac{4k\lambda_{k;\gamma}}{(\lambda_{k;\gamma}^2 + k^2)^2}, & g_{4,k} &= \frac{2k(k^2 - 3\lambda_{k;\gamma}^2)}{(k^2 + \lambda_{k;\gamma}^2)^3} \\ g_{5,k} &= \frac{8k\lambda_{k;\gamma}(k^2 - \lambda_{k;\gamma}^2)}{(k^2 + \lambda_{k;\gamma}^2)^4}, & g_{6,k} &= -\frac{2k(5\lambda_{k;\gamma}^4 - 10k^2\lambda_{k;\gamma}^2 + k^4)}{(k^2 + \lambda_{k;\gamma}^2)^5}. \end{aligned} \tag{21}$$

Note that q_2 is the Bethe state energy eigenvalue and is given in (13). It is also interesting to observe that $g_{n,k}$ (cf. (21)) is vanishing for infinite BGT roots. This is expected to hold for the generic $g_{n,k}$, i.e., for any n, and it is a consequence of the $SU(2)$ invariance of the conserved charges. Finally, in the thermodynamic limit $L \to \infty$ from (20) one has

$$q_n \to \sum_{k=1}^{\infty} \int_{-\infty}^{+\infty} d\lambda \rho_k(\lambda) g_{n,k}(\lambda), \tag{22}$$

where the BGT root distributions $\rho_k(\lambda)$ are solutions of (14).

3. Overlap between the Bethe states and some initial states

Here we detail the Bethe ansatz results for the overlap of the Bethe states (cf. (3)) with the zero-momentum (one-site shift invariant) Néel state $|N\rangle$ and the Majumdar-Ghosh (MG) $|MG\rangle$ state. We stard discussing the Néel state. This is defined as

$$|N\rangle \equiv \frac{1}{\sqrt{2}}(|N_1\rangle + |N_2\rangle), \tag{23}$$

with $|N_1\rangle \equiv |\uparrow\downarrow\rangle^{\otimes L/2}$, and $|N_2\rangle \equiv |\downarrow\uparrow\rangle^{\otimes L/2}$. Note that $|N_1\rangle = \hat{T}|N_2\rangle$, with $\hat{T}$ the one-site shift operator.

Due to the zero-momentum constraint, only parity-invariant Bethe states can have non-zero Néel overlap [6]. Parity-invariant Bethe states contain only pairs of solutions of the Bethe equations (7) with opposite sign. Here we denote the generic parity-invariant rapidity configuration as $|\{\pm\tilde{\lambda}_\alpha\}_{\alpha=1}^m, n_\infty\rangle$, i.e., considering only positive rapidities. Here m is the number of rapidity pairs. Since the Néel state is not invariant under $SU(2)$ rotations, eigenstates with infinite rapidities can have non-zero Néel overlaps. Here the number of infinite rapidities is denoted as N_∞. Note that one has $M = L/2 = N_\infty + 2m$. We denote as $n_\infty \equiv N_\infty/L$ the density of infinite rapidities. Finally, the overlap between the Bethe states and the Neel state $|N\rangle$ reads [6, 11]

$$\frac{\langle N|\{\pm\tilde{\lambda}_j\}_{j=1}^m, n_\infty\rangle}{|||\{\tilde{\lambda}_j\}_{j=1}^m, n_\infty\rangle||} = \frac{\sqrt{2}N_\infty!}{\sqrt{(2N_\infty)!}} \left[\prod_{j=1}^m \frac{\sqrt{\tilde{\lambda}_j^2+1}}{4\tilde{\lambda}_j}\right] \sqrt{\frac{\det_m(G^+)}{\det_m(G^-)}}. \tag{24}$$

The matrix $G^\pm$ is defined as

$$G^\pm_{jk} = \delta_{jk}\Big(LK_{1/2}(\tilde{\lambda}_j) - \sum_{l=1}^m K_1^+(\tilde{\lambda}_j, \tilde{\lambda}_l)\Big) + K_1^\pm(\tilde{\lambda}_j, \tilde{\lambda}_k), \quad j,k = 1,\ldots,m, \tag{25}$$

where

$$K_1^\pm(\lambda,\mu) = K_1(\lambda-\mu) \pm K_1(\lambda+\mu) \quad \text{with} \quad K_\alpha(\lambda) \equiv \frac{8\alpha}{\lambda^2+4\alpha^2}. \tag{26}$$

Note that our definitions of $K_\alpha(\lambda)$ differs from the one in Ref. [6], due to a factor 2 in the definition of the rapidities (see also (10)).

3.1. The string hypothesis: Reduced overlap formulas

Here we consider the overlap formula for the Neel state (24) in the limit $L \to \infty$, assuming that the rapidities form perfect strings, i.e., $\delta^j_{n;\gamma} = 0$ in (10). Then it is possible to rewrite (24) in terms of the string centers $\tilde{\lambda}_{n;\alpha}$ only. Here we restrict ourselves to rapidity configurations with no zero-momentum strings, i.e., with finite string centers. Our results are not valid for zero-momentum strings.

First, we restrict ourselves to parity-invariant string configurations, i.e., considering only strings having positve string centers. We denote the generic parity-invariant string configuration as $\{\tilde{\lambda}_{n;\gamma}\}$, where γ labels the different non-zero string centers, and n is the string length.

It is convenient to first split the indices i, j of $G^{\pm}_{ij}$ as $i = (n, \gamma, i)$ and $j = (m, \gamma', j)$, with n, m being the length of the strings, γ, γ' labelling the corresponding string centers, and i, j the components of the two strings.

Using (25) and (26), one has that for two consecutive rapidities in the same string, i.e., for $m = n, \gamma = \gamma', |i - j| = 2$, the matrices $G^{\pm}_{jk}$ become ill-defined in the thermodynamic limit. Precisely, since $K_1(\tilde{\lambda}^i_{n;\gamma} - \tilde{\lambda}^{i+1}_{n;\gamma}) \sim 1/(\delta^i_{n;\gamma} - \delta^{i+1}_{n;\gamma})$, $G^{\pm}_{ij}$ diverges in the thermodynamic limit. Importantly, as the same type of divergence occur in both G^+ and G^-, their ratio (cf. (24)), and the overlaps, are finite.

The finite part of the overlaps (24) can be calculated using the same strategy as in Ref. [8, 9] (see also Ref. [6]). The resulting matrix G^+ depends only on the "string center" indices (n, γ) and (m, γ') and it is given as

$$\frac{1}{2}G^+_{(n,\gamma)(m,\gamma')} = \begin{cases} L\theta'_n(\tilde{\lambda}_{n;\gamma}) - \sum\limits_{(\ell,\alpha)\neq(n,\gamma)} \Big[\Theta'_{n,\ell}(\tilde{\lambda}_{n;\gamma} - \tilde{\lambda}_{\ell;\alpha}) & \text{if } (n,\gamma) = (m,\gamma') \\ \qquad +\Theta'_{n,\ell}(\tilde{\lambda}_{n;\gamma} + \tilde{\lambda}_{\ell;\alpha})\Big] & \\ \Theta'_{n,m}(\tilde{\lambda}_{n;\gamma} - \tilde{\lambda}_{m;\gamma'}) + \Theta'_{n,m}(\tilde{\lambda}_{n;\gamma} + \tilde{\lambda}_{m;\gamma'}) & \text{if } (n,\gamma) \neq (m,\gamma') \end{cases} \tag{27}$$

Here $\theta'_n(x) \equiv d\theta_n(x)/dx = 2n/(n^2 + x^2)$ and $\Theta'(x) \equiv d\Theta(x)/dx$, with $\Theta(x)$ as defined in (12). Similarly, for G^- one obtains

$$\frac{1}{2}G^-_{(n,\gamma)(m,\gamma')} = \begin{cases} (L-1)\theta'_n(\tilde{\lambda}_{n;\gamma}) - 2\sum\limits_{k=1}^{n-1}\theta'_k(\tilde{\lambda}_{n;\gamma}) & \text{if } (n,\gamma) = (m,\gamma') \\ -\sum\limits_{(\ell,\alpha)\neq(n,\gamma)} \Big[\Theta'_{n,\ell}(\tilde{\lambda}_{n;\gamma} - \tilde{\lambda}_{\ell;\alpha}) + \Theta'_{n,\ell}(\tilde{\lambda}_{n;\gamma} + \tilde{\lambda}_{\ell;\alpha})\Big] & \\ \Theta'_{n,m}(\tilde{\lambda}_{n;\gamma} - \tilde{\lambda}_{m;\gamma'}) - \Theta'_{n,m}(\tilde{\lambda}_{n;\gamma'} + \tilde{\lambda}_{m;\gamma'})) & \text{if } (n,\gamma) \neq (m,\gamma') \end{cases} \tag{28}$$

Note that in presence of zero-momentum strings, additional divergences as $1/(\delta^i_{n;\gamma} + \delta^{i+1}_{n;\gamma})$ appear due to the term $K_1(\lambda + \mu)$ (cf. (26)). It turns out that the treatment of these diverges is a challenging task because it requires the precise knowledge of the string deviations, meaning their dependence on L, for each different type of string. Some results have been provided for small strings in Ref. [1].

Finally, using the string hypothesis and the parity-invariance condition, the multiplicative prefactor in (24) can be simplified. Here we focus on a generic eigenstate

of the XXX identified by m pairs of finite rapidities. Note that due to parity invariance and the exclusion of zero-momentum strings, only strings of length up to m are allowed. The "reduced" string content identifying the eigenstate is denoted as $\widetilde{\mathcal{S}} = \{\tilde{s}_1, \ldots, \tilde{s}_m\}$, with $\tilde{s}_n$ the number of parity-invariant pairs of n-strings. Using the string hypothesis and (24), one can write

$$\prod_{j=1}^{m} \frac{\sqrt{\tilde{\lambda}_j^2+1}}{4\tilde{\lambda}_j} = \frac{1}{4^m} \prod_{j=1}^{m} \prod_{\ell=1}^{\tilde{s}_j} \left[\frac{\sqrt{j^2+\lambda_{j;\ell}^2}}{\lambda_{j;\ell}} \prod_{k=0}^{\lceil j/2 \rceil - 1} \frac{(2k)^2+\lambda_{j;\ell}^2}{(2k+1)^2+\lambda_{j;\ell}^2} \right]^{(-1)^j} . \tag{29}$$

3.2. Thermodynamic limit

In the thermodynamic limit $L \to \infty$ the expression for the extensive part of the overlap (24) can be written as [6]

$$-\lim_{L\to\infty} \log \left[\frac{\langle N | \{\pm\lambda_j\}_{j=1}^m, n_\infty \rangle}{|||\{\lambda_j\}_{j=1}^m, n_\infty \rangle||} \right] = \frac{L}{2} \Big(n_\infty \log 2 + \sum_{n=1}^{\infty} \int_0^\infty d\lambda \rho_n(\lambda) [g_n(\lambda) + 2n \log(4)] \Big), \tag{30}$$

where

$$g_n(\lambda) = \sum_{l=1}^{n-1} \Big[f_{n-1-2l}(\lambda) - f_{n-2l}(\lambda) \Big], \quad \text{with} \quad f_n(\lambda) = \log\left(\lambda^2 + \frac{n^2}{4}\right), \tag{31}$$

and

$$n_\infty = 1 - 2 \sum_{m=1}^{\infty} m \int_{-\infty}^{\infty} d\lambda \rho_m(\lambda). \tag{32}$$

Note that (30) is extensive. Specifically, in Eq. (30) subleading (i.e., subextensive) contributions originating from the determinant ratio $\det_m(G^+)/\det_m(G^-)$ are neglected.

4. Overlap with the Majumdar-Ghosh state

The Majumdar-Ghosh state $|MG\rangle$ is defined as

$$|MG\rangle \equiv \left(\frac{|\uparrow\downarrow\rangle - |\downarrow\uparrow\rangle}{\sqrt{2}} \right)^{\otimes L/2}. \tag{33}$$

The overlap between a generic eigenstate of the XXX chain and the Majumdar-Ghosh state can be obtained from the Néel state overlap in Eq. (24) as [11]

$$\langle MG | \{\pm\lambda_j\}_{j=1}^m \rangle = \prod_{j=1}^{m} \frac{1}{2} \Big(1 - \frac{\lambda_j - i}{\lambda_j + i}\Big) \Big(1 + \frac{\lambda_j + i}{\lambda_j - i}\Big) \langle N | \{\pm\lambda_j\}_{j=1}^m \rangle \tag{34}$$

The mutliplicative factor in (**??**), using the string hypothesis for the generic n-string is rewritten as

$$\prod_{j=1}^{M} \frac{1}{\sqrt{2}} \Big(1 - \frac{\lambda_j - i}{\lambda_j + i}\Big) = 2^n \prod_{k=0}^{\lfloor n/2 \rfloor} \frac{1}{[\lambda_{n;\gamma}^2 + (2k + (1-(-1)^n)/2)^2]^2} \tag{35}$$

5. Quench Action method

For integrable models the Quench-Action approach allows to extract exactly both the steady state after the quench and the relaxation dynamics to the steady state.
In the thermodynamic limit the sum over the model eigenstates is recast into a functional integral over the so-called root distributions $\boldsymbol{\rho} \equiv \{\rho_n(\lambda)\}_{n=1}^{\infty}$ as

$$\sum_{\alpha} \to \int \mathcal{D}\boldsymbol{\rho} e^{S_{YY}(\boldsymbol{\rho})}. \tag{36}$$

Here $\mathcal{D}\boldsymbol{\rho} \equiv \prod_{n=1}^{\infty} \mathcal{D}\rho_n(\lambda)$, $\rho_n(\lambda)$ denote the distribution of the n-strings BGT roots, and $S_{YY}(\boldsymbol{\rho})$ is the Yang-Yang entropy, which counts the number of Bethe states leading to the same $\boldsymbol{\rho}$ in the thermodynamic limit. Formally, $\rho_n(\lambda)$ are defined as $\rho_n(\lambda) \equiv \lim_{L\to\infty}(\lambda_{n;\gamma+1} - \lambda_{n;\gamma})^{-1}$.
Using (36) the diagonal ensemble (1) becomes

$$\langle \mathcal{O} \rangle = \int \mathcal{D}\boldsymbol{\rho}(\lambda) \exp\Big(2\Re \log\langle \Psi_0|\boldsymbol{\rho}(\lambda)\rangle + S_{YY}(\boldsymbol{\rho})\Big) \langle \boldsymbol{\rho}(\lambda)|\mathcal{O}|\boldsymbol{\rho}(\lambda)\rangle \tag{37}$$

Note that in (37) it is assumed that in the thermodynamic limit the eigenstate expectation values $\langle\alpha|\mathcal{O}|\alpha\rangle$ become smooth functionals $\langle\boldsymbol{\rho}(\lambda)|\mathcal{O}|\boldsymbol{\rho}(\lambda)\rangle$ of the root distributions $\boldsymbol{\rho}$.
Similarly, in (37) $\langle\Psi_0|\boldsymbol{\rho}(\lambda)\rangle$ denotes the Bethe states overlap density with the prequench state Ψ_0.
The strategy is to evaluate the functional integral in (37) using the saddle point approximation.
One has then to minimize the functional $\mathcal{S}(\boldsymbol{\rho})$ defined as

$$L\mathcal{S}(\boldsymbol{\rho}) \equiv 2\Re \log\langle\boldsymbol{\rho}|\Psi_0\rangle + S_{YY}(\boldsymbol{\rho}(\lambda)). \tag{38}$$

under the constraint that the BGT equations hold. For the quench with initial state the Néel state the resulting saddle point root distributions $\rho_n^*(\lambda)$ can be obtained analytically. The first few root distributions are given as

$$\rho_1^*(\lambda) = \frac{8(4+\lambda^2)}{\pi(19+3\lambda^2)(1+6\lambda^2+\lambda^4)} \tag{39}$$

$$\rho_2^*(\lambda) = \frac{8\lambda^2(9+\lambda^2)(4+3\lambda^2)}{\pi(2+\lambda^2)(16+14\lambda^2+\lambda^4)(256+132\lambda^2+9\lambda^4)} \tag{40}$$

$$\rho_3^* = \frac{8(1+\lambda^2)^2(5+\lambda^2)(16+\lambda^2)(21+\lambda^2)}{\pi(19+3\lambda^2)(9+624\lambda^2+262\lambda^4+32\lambda^6+\lambda^8)(509+5\lambda^2(26+\lambda^2))}. \tag{41}$$

6. Overlap sum rules: the role of the zero-momentum strings

In this section we investigate the role of the zero-momentum strings. We focus on conserved quantities sum rules. Specifically, given a generic conserved quantity (charge) $\hat{Q}$ we consider the trivial identity

$$Q_0 \equiv \langle\Psi_0|\hat{Q}|\Psi_0\rangle = \sum_{\lambda} |\langle\lambda|\Psi_0\rangle|^2 Q_\lambda, \tag{42}$$

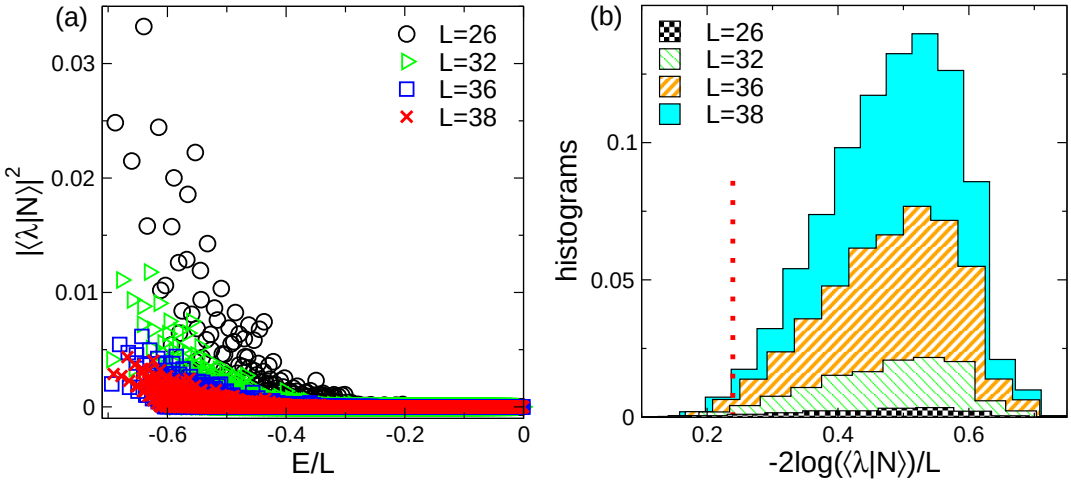

Figure 1. Néel state overlaps in the Heisenberg spin chain. (a) The Néel state overlaps with the eigenstates of the Heisenberg spin chain: Squared overlaps $|\langle\lambda|N\rangle|^2$ plotted as a function of the eigenstates energy density E/L. Here $|\lambda\rangle$ denotes the generic eigenstate of the Heisenberg spin chain. The data are for chains with length $26 \leq L \leq 38$. The data are obtained from a full scanning of the chains Hilbert space. Eigenstates containing strings with zero-momentum components are escluded. The overlaps decay exponentially with the chain size. (b) Histograms of $-2\log|\langle\lambda|N\rangle|/L$. Different histograms are for different chain sizes. The histogram bin width is $\sim 2/L$. The y-axis is rescaled by a factor 10^5 for convenience. Note the peaking of the histograms around $-2\log|\langle\lambda|N\rangle| \sim 0.5$ in the thermodynamic limit **really??**. The dotted vertical line is the expected Quench-Action result in the thermodynamic limit.

where Q_0 is the charge expectation values over the initial state $|\Psi_0\rangle$, $|\lambda\rangle$ denotes the generic eigenstate of the XXX chain, and Q_λ is the charge eigenvalue over the eigenstate.

Here we restrict ourselves to the cases with $\hat{Q} = \mathbb{I}$ and $\hat{Q} = \mathcal{H}$, considering both the case with $|\Psi\rangle = |N\rangle$ and $|\Psi_0\rangle = |MG\rangle$.

For the Néel state, for any finite L Eq. (42) gives $Q_0 = 1, -1/2$ for $\hat{Q} = \mathbb{I}$ and $\hat{Q} = \mathcal{H}$, respectively.

Figure 2 plots the numerical results obtained via a full scanning of the Hilbert space of the Heisenberg chain.

Precisely, the numerical data are obtained by generating all the possible string contents $\mathcal{S}$ compatible with the parity-invariance constraint

Panel (a) and (b) in the Figure plots the sum rule (42) for $\hat{Q} = \mathbb{I}$ and $\hat{Q} = \mathcal{H}$, respectively. The circles are obtained considering all the eigenstates of the Heisenberg spin chain with L sites, excluding eigenstates containing zero-momentum strings.

The total number of eigenstates $\widetilde{Z}_{Neel}$ containing no zero-momentum strings is given as

$$\widetilde{Z}_{Neel} = B\Big(\frac{L}{2}, \frac{L}{4}\Big). \tag{43}$$

The proof of(43) is reported in Appendix B.

The largest chain size considered is $L = 36$. The data are plotted versus $1/L$.

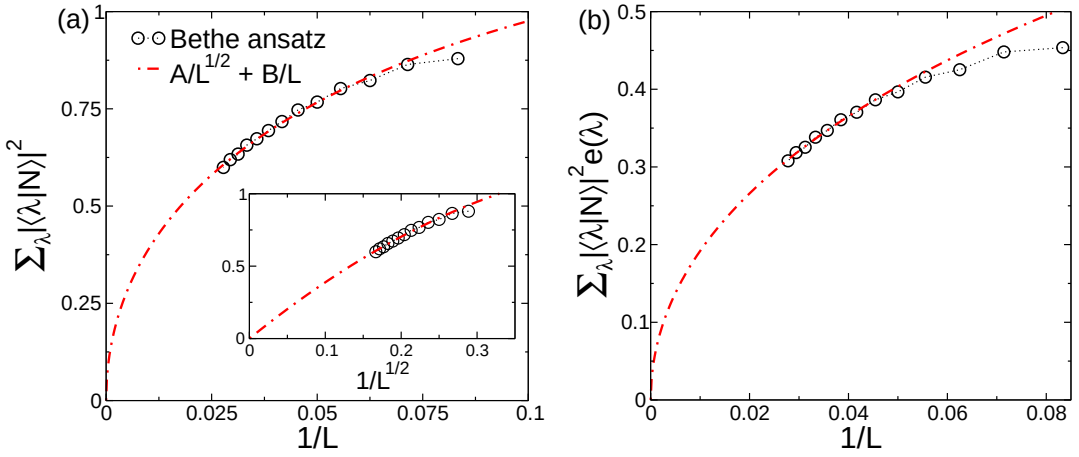

Figure 2. Overlap sum rules for the Neel state: The role of the zero-momentum strings. (a) The overlap sum rule $\sum_\lambda |\langle\lambda|N\rangle|^2 = 1$, with $|N\rangle$ the Neel state and $|\lambda\rangle$ the eigenstates of the XXX spin chain. The x-axis shows $1/L$, with L the chain length. The circles are Bethe ansatz results for chains up to $L = 36$. The results are obtained via a full scanning of the chain Hilbert space. Only the eigenstates with no zero-momentum strings are considered. The dash-dotted line is a fit to $A/L^{1/2} + B/L$, with A, B fitting parameters. Inset: The same data as in the main Figure plotted versus $1/L^{1/2}$. (b) The same as in (a) for the sum rule $\sum_\lambda |\langle\lambda|N\rangle|^2 e(\lambda) = 1/2$, with $e(\lambda)$ the eigenstates energy density.

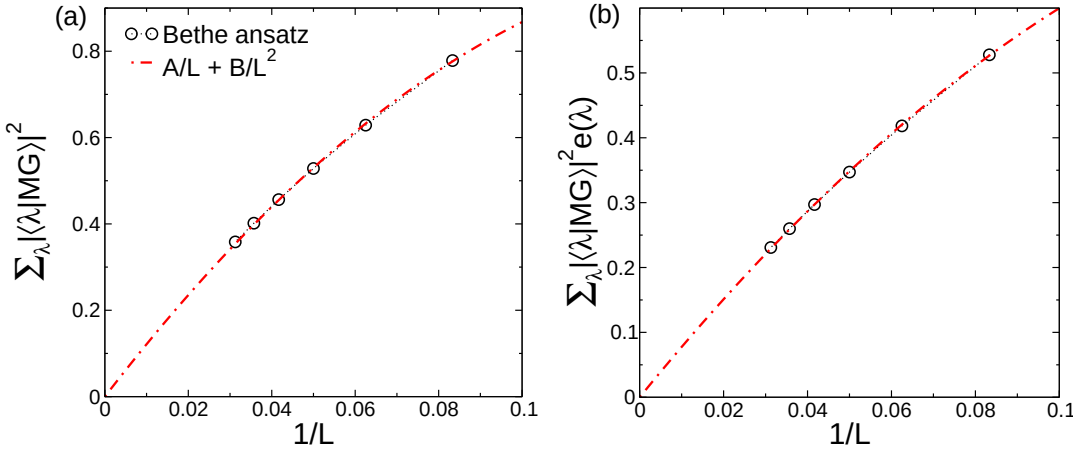

Figure 3. Overlap sum rules for the Majumdar-Ghosh (MG) state. (a) The overlap sum rule $\sum_\lambda |\langle\lambda|MG\rangle|^2 = 1$, with $|MG\rangle$ the Majumdar-Ghosh state and $|\lambda\rangle$ the eigenstates of the XXX spin chain. The x-axis shows $1/L$, with L the chain length. The circles are Bethe ansatz results for chains up to $L = 36$. The results are obtained via a full scanning of the chain Hilbert space. Only the eigenstates with no zero-momentum strings are considered. The dash-dotted line is a fit to $A/L + B/L^2$, with A, B fitting parameters. (b) The same as in (a) for the sum rule $\sum_\lambda |\langle\lambda|MG\rangle|^2 e(\lambda) = 2/3$, with $e(\lambda) \equiv E/L$ the eigenstates energy density.

Interestingly, both the sum rules (panels (a)(b)) are not saturated, as expected since the eigenstates corresponding to zero-momentum strings are excluded in the sum in the

right-hand-side in (42).
Interestingly, both sum rules exhibit vanishing behavior upon increasing the chain size. The dash-dotted lines in the Figures are fits to the behavior $A/L^{1/2} + B/L$, with A, B fitting parameters, and perfectly describe the behavior of the data.
The vanishing behavior as $\propto 1/L^{1/2}$ of the sum rules reflects the vanishing of the fraction of non-zero momentum string eigenstates in the thermodynamic limit ad

$$\frac{\widetilde{Z}_{Neel}}{Z_{Neel}} \propto \frac{4}{\sqrt{\pi L}}, \tag{44}$$

with Z_{Neel} being the total number of eigenstates corresponding to parity invariant BGT quantum numbers configurations.
One should observe that the asymptotic, i.e., at large L, behavior (44) is not generic, meaning that different initial states $|\Psi_0\rangle$ might give different behaviors.
This is illustrated in Figure 3, focusing on the Majumdar-Ghosh (MG) state. Panels (a) and (b) plot the sum rules with $\hat{Q} = \mathbb{I}$ and $\hat{Q} = \mathcal{H}$ (same as in Figure 2). As for the Néel state only eigenstates containing no zero-momentum strings are consdidered. Note that their number $\widetilde{Z}_{MG}$ (see Appendix B) is now given as

$$\widetilde{Z}_{MG} = B\Big(\frac{L}{2}, \frac{L}{4}\Big) - B\Big(\frac{L}{2}, \frac{L}{4} - 1\Big). \tag{45}$$

Similar to Figure 2, due to the exclusion of the zero-momentum strings, the saturation rules exhibit vanishing behavior in the thermodynamic limit. However, in contrast with the Néel case (see Figure 2), one has the behavior $Q_0 \sim 1/L$, as confirmed by the fits (dash-dotted lines in Figure 3).
Similar to the Néel case this reflects the same vanishing behavior of the eigenstates containing no zero-momentum strings $\widetilde{Z}_{MG}/Z_{MG}$ as

$$\frac{\widetilde{Z}_{MG}}{Z_{MG}} = \frac{4}{4 + L}. \tag{46}$$

7. Monte Carlo implementation of the Quench-Action approach

For the finite-size Heisenberg spin chain the Quench-Action expectation values can be obtained by sampling the eigenstates of the chain using Monte Carlo. One starts with an eigenstate of the XXX chain with N_∞ infinite rapidities and $M \equiv L/2 - N_\infty$ finite ones. The state is identified by a parity-invariant Bethe quantum number configuration $\mathcal{C}$ and by the corresponding parity-invariant rapidities $\{\lambda\}$ as $|\lambda\rangle$. The string content associated with the finite rapidities is denoted as $\mathcal{S}$. The Monte Carlo procedure consists of four steps as follows:

(1) Choose a new number of finite rapidities M' with probability

$$\mathcal{P}(M') = \frac{\widetilde{Z}'_{Neel}(L, M')}{\widetilde{Z}_{Neel}(L)}. \tag{47}$$

(2) Choose a new a new string content $\mathcal{S}' \equiv \{s'_1, \ldots, s'_{M'}\}$ with probability $\mathcal{P}'(M', \mathcal{S}')$

$$\mathcal{P}'(M', \mathcal{S}') = \frac{1}{\widetilde{Z}'_{Neel}(L, M')} \prod_{n=1}^{M'} B\Big(\frac{L}{2} - \frac{1}{2}\sum_{m=1}^{M'} t_{nm} s'_m, s'_n\Big). \tag{48}$$

(3) Generate a new parity-invariant quantum number configuration $\mathcal{C}'$ compatible with the $\mathcal{S}'$ obtained in step (2). Solve the corresponding BGT equations (**??**), finding a new eigenstate $|\lambda'\rangle$.

(4) Calculate the overlap $\langle\lambda'|N\rangle$ between the new eigenstate and the Néel state and accept the eigenstate with the Metropolis probability

$$\mathcal{P}''_{\lambda\to\lambda'} = \mathrm{Min}\Big\{1, \exp\Big(-2\Re(\mathcal{E}' - \mathcal{E})\Big)\Big\}, \tag{49}$$

where $\mathcal{E}' \equiv -\log\langle\lambda'|N\rangle$, similarly for $\mathcal{E}$, and $\Re$ denotes the real part.

Afte some necessary thermalization steps the sequence $1-4$ generates eigenstates of the XXX chain distributed according to the Quench-Action probability distribution.
For a generic observable $\mathcal{O}$, its Quench-Action expectation value $\langle\mathcal{O}\rangle_{QA}$ is obtained as the arithmetic average of the expectation value over the eigenstates sampled in the Monte Carlo as

$$\langle\mathcal{O}\rangle_{QA} = \frac{1}{N_{mcs}} \sum_{\lambda} \langle\lambda|\mathcal{O}|\lambda\rangle, \tag{50}$$

with N_{mcs} being the total number of Monte Carlo steps.

8. Monte Carlo Quench-Action approach: Numerical results

In this section we numerically demonstrate that the only effect of neglecting the zero-momentum strings are finite-size corrections.
The validity of the Monte Carlo approach for simulating the Quench-Action results is demonstrated in Figure 4. The Figure focuses on the Néel sum rules for the conserved charges Q_2 and Q_4. Specifically, panel (a) shows the sum rules for $\hat{Q} = \hat{Q}_2$, $\hat{Q} = \hat{Q}_4$, and the corresponding fluctuations $\sigma^2(Q_n) \equiv \langle N|\hat{Q}_n^2|N\rangle - \langle N|\hat{Q}_n|N\rangle^2$.

$$\langle N|\hat{Q}_n|N\rangle = \sum_{\lambda} |\langle N|\lambda\rangle|^2 Q_n. \tag{51}$$

Note that the Néel sum rule for the identity $\mathbb{I}$ is trivially satisfied, and it corresponds to the normalization of the Monte Carlo probability. Figure 4 (a) plots the Néel sum rule for the energy density Q_2/L. The circles are Monte Carlo data obtained using the procedure outlined in 7 for several Heisenberg spin chains. The largest chain simulated is for $L = 56$ sites. The data correspond to a simulation with $\sim 10^7$ Monte Carlo step (mcs). The expected result $\langle N|\hat{Q}_2|N\rangle/L = -1/2$ is shown as dash-dotted line.
In stark contrast with Figure 2 and Figure 3, while for small chains the sum rule is violated the data strongly suggest that in the thermodynamic limit the sum rule saturates the expected theoretical value.

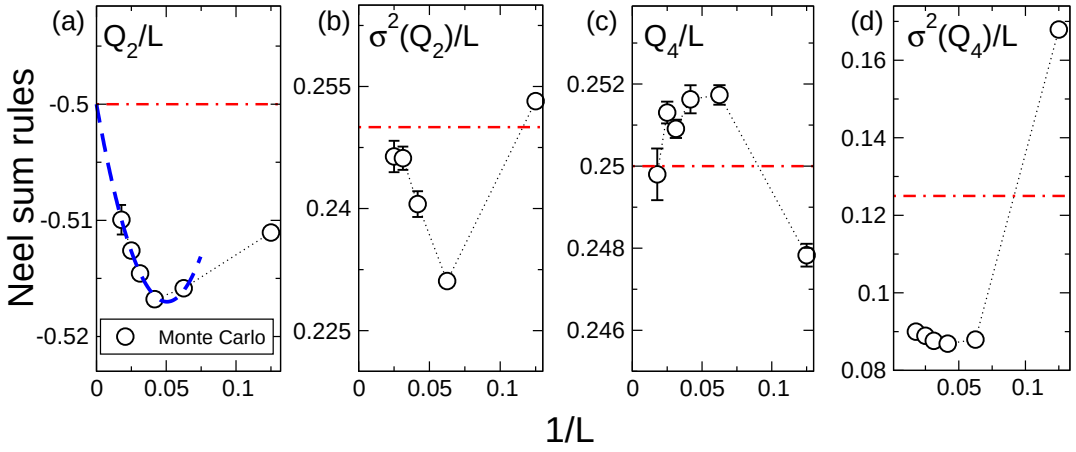

Figure 4. The overlap sum rules for the Neel state: Numerical results obtained using the Hilbert space Monte Carlo sampling approach. (a) The energy sum rule $\langle N|Q_2|N\rangle/L = -1/2$, with Q_2/L the Hamiltonian density. We plot $\sum_\lambda |\langle\lambda|N\rangle|^2 Q_2(\lambda)/L = 1/2$, with $|\lambda\rangle$ the eigenstates of the XXX chain, versus the inverse chain length $1/L$. The symbols are Monte Carlo data obtained by sampling the eigenstates of the XXX chain. The dash-dotted line is the expected result. The dashed line is a fit to the behavior $-1/2 + A/L + B/L^2$, with A, B fitting parameters. (b) The energy fluctuations sum rule $\sigma^2(Q_2)/L \equiv (\langle N|Q_2^2|N\rangle - \langle N|Q_2|N\rangle^2)/L = 1/4$. The horizontal line is the expected result. (c)(d) Same as in (a)(b) for the charge Q_4 and its fluctuations.

Furthermore, the data suggest the behavior $\propto 1/L$, as confirmed by the fit to $-1/2 + A/L + b/L^2$ (dashed line in the Figure), with A, B fitting parameters.
The same qualitative behavior is demonstrated in panel (b) for the energy fluctuations. Interestingly, for $L = 56$ the Monte Carlo result is compatible within the error bar with the expected asymptotic one.
Finally, panels (c)(d) show the same results as for (a)(b) for the conserved charge Q_4.

9. The Quench-Action root distributions

The BGT root distributions $\rho_n(\lambda)$ identifying the Quench-Action saddle point can be extracted from the Monte Carlo simulation as shown in [2].
Figure 5 displays the first two root distributions $\rho_1(\lambda)$ (panel (a)) and $\rho_2(\lambda)$ (panel (b)), plotted agains the BGT root λ. The data are the histograms of the BGT roots sampled in the Monte Carlo. The data are for a chain with $L = 56$ sites and $N_{mcs} \sim 10^7$ Monte Carlo steps. All the data are divided by a factor 10^6 for plotting convenience. The width of the histogram bins $\Delta\lambda$ is $\Delta\lambda \approx 0.02$ and $\Delta\lambda \approx 0.001$ for $\rho_1(\lambda)$ and $\rho_2(\lambda)$, respectively.
The histogram fluctuations are due to N_{mcs} being finite, and are expected to vanish in the limit $N_{mcs} \to \infty$.
The continuous lines is the expected analytic result in the thermodynamic limit.
Clearly, $\rho_1(\lambda)$ is in good agreement with the Monte Carlo data in the whole range

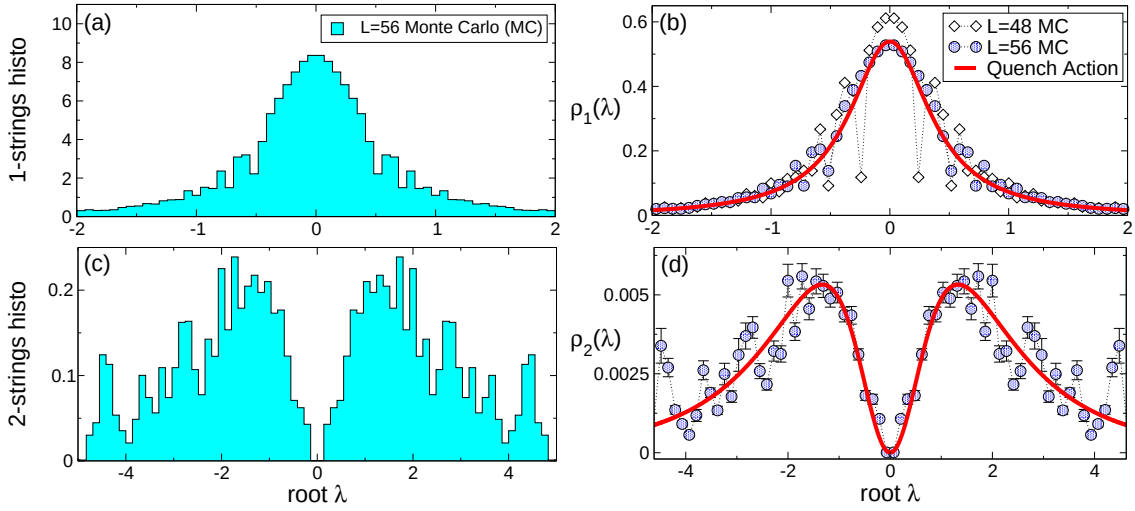

Figure 5. The Quench-Action steady state root ddistributions $\rho_1(x)$ and $\rho_2(x)$: Monte Carlos results. (a) The histograms of the 1-string rapidities sampled in the Monte Carlo. The x-axis shows the 1-string BGT root λ. The data are for a chain with $L = 56$ sites and $N_{mcs} \sim 10^7$ Monte Carlo steps. The data are divided by a factor 10^6 for plotting convenience. The width of the histogram bin is $\Delta\lambda \sim 0.07$. (b) The same as in (a) for the 2-string roots sampled in the Monte Carlo. (b) The extracted 1-string root distribution $\rho_1(\lambda)$ plotted versus λ for two chains with $L = 48$ and $L = 56$ (diamond and circles, respectively). The full line is the Quench-Action analytic result in the thermodynamic limit. (d) The same as in (c) for the 2-string root density $\rho_2(\lambda)$. In both (c)(d) the oscillations are finite-size effects, whereas the error bars show the statistical Monte Carlo error.

$-2 \leq \lambda \leq 2$ considered. On the other hand, larger deviations from the theoretical result are present for $\rho_2(\lambda)$. These deviations are larger on the tails of the distribution. This is expected since large λ correspond to large quasimomenta, which are more sensitive to the finite size of the chain.

9.1. Counting of eigenstates with non-zero Neel overlap

We numerically checked that the number of states with non-zero overlap with the Neel state is given as

$$Z_{Neel} = 2^{\frac{L}{2}-1} + \frac{1}{2}B\left(\frac{L}{2}, \frac{L}{4}\right) + 1, \tag{52}$$

with $B(x, y)$ denoting the binomial coefficient. The contribution 1 accounts for the ferromagnetic state. Here we assumed that L is divisible by four. Here Z_N is be obtained as the total number of parity-invariant Bethe-Gaudin-Takahashi quantum numbers. After excluding the zero-momentum strings the total number of states with non-zero overlap with the Neel state is

$$\widetilde{Z}_{Neel} = \left(\frac{L}{2}, \frac{L}{4}\right) \tag{53}$$

Importantly, the fraction of eigenstates corresponding to non-zero momentum strings is vanishing in the thermodynamic limit as

$$\frac{\widetilde{Z}_{Neel}}{Z_{Neel}} \propto \frac{4}{\sqrt{\pi L}}. \tag{54}$$

Appendix A. Eigenstates with nonzero Néel overlap: eigenstates counting and string content

Here we prove that the total number of eigenstates with Néel nozero overlap $Z_{Neel}(L)$for a chain of length L is given as

$$Z_{Neel} = 2^{\frac{L}{2}-1} + \frac{1}{2}B\Big(\frac{L}{2},\frac{L}{4}\Big) + 1. \tag{A.1}$$

For simplicity here we restrict ourselves to the situation with L divisible by four. The strategy to prove (A.1) is to count all the possible parity-invariant BGT quantum numbers configurations. Let us consider the sector with fixed number of particles M, and a generic string content $\mathcal{S} = \{s_1, s_2, \ldots, s_M\}$. Here s_n is the number of n-strings, and one has the constraint $\sum_k k s_k = M$.

It is straightforward to check that total number of parity-invariant quantum number pairs $\mathcal{N}_n(L,\mathcal{S})$ in the n-string sector is given as

$$\mathcal{N}_n(L,\mathcal{S}) = \Big\lfloor \frac{L}{2} - \frac{1}{2}\sum_{m=1}^{M} t_{nm}s_m \Big\rfloor. \tag{A.2}$$

where $t_{nm} \equiv 2\mathrm{Min}(n,m) - \delta_{n,m}$. The number of parity-invariant quantum number configurations (i.e., eigenstates) $\mathcal{N}(L,\mathcal{S})$ compatible with string content $\mathcal{S}$ is obtained by choosing in all the possible ways the parity-invariant quantum number pairs independently in each n-string sector, which implies that

$$\mathcal{N}(L,\mathcal{S}) = \prod_{m=1}^{M} B\left(\mathcal{N}_m, \Big\lfloor \frac{s_m}{2} \Big\rfloor\right). \tag{A.3}$$

Here the product is because each string sector is treated independently, while the factor $1/2$ in $s_m/2$ is because since all quantum numbers are organized in pairs, only half of the quantum numbers have to be specified. Note that in each n-string sector only one zero momentum (i.e., zero quantum number) string is allowed, due to the Pauli principle. Moreover, s_m is odd (even) only if the zero momentum string is (not) present. The floor function $\lfloor\cdot\rfloor$ in (A.3) reflects that the quantum number of zero-momentum strings is fixed.

We now consider the string configurations with particle number $0 \leq \ell \leq M$ and fixed number of strings $1 \leq q \leq M/2$. Note that the maximul allowed string length is $M/2$ beacause of parity invariance. Note also that in determining q strings of different length are treated equally. Clearly, one has that $\sum_m s_m = q$. For a given fixed pair ℓ, q the total number of quantum number configurations is given as

$$\mathcal{N}'(L,\ell,q) = \sum_{\{\{s_m\}:\sum m s_m=\ell,\sum s_m=q\}} \mathcal{N}(L,\mathcal{S}), \tag{A.4}$$

where the sum is over the content $\{s_m\}_{m=1}^M$ compatible with the constraints $\sum_m s_m = q$ and $\sum_m m s_m = \ell$. The strategy is to write a recursive relation for $\mathcal{N}'(L,\ell,q)$. To this purpose it is useful to consider the shifted string content $\mathcal{S}'$ defined as

$$\mathcal{S}' \equiv \{s_{m+1}\} \quad \text{with } s_m \in \mathcal{S},\ \forall m. \tag{A.5}$$

Using the definition of t_{ij}, it is straightforward to derive that

$$t_{ij} = t_{i-1,j-1} + 2, \tag{A.6}$$

which implies that $\mathcal{N}_n(L,\mathcal{S})$ (see (A.2)) satisfies the recursive equation

$$\mathcal{N}_n(L,\mathcal{S}) = \mathcal{N}_{n-1}(L-2q,\mathcal{S}'). \tag{A.7}$$

After substituting in (A.3) one obtains

$$\mathcal{N}(L,\mathcal{S}) = B\Big(\mathcal{N}_1(L,\mathcal{S}), \Big\lfloor \frac{s_1}{2} \Big\rfloor\Big)\mathcal{N}(L-2q,\mathcal{S}'). \tag{A.8}$$

Finally, after substituting (A.8) in (A.4), one obtains a recursive relation for $\mathcal{N}'(L,\ell,q)$ as

$$\mathcal{N}'(L,\ell,q) = \sum_{s=0}^{q-1} B\Big(\frac{L}{2} - q + \Big\lfloor \frac{s}{2} \Big\rfloor, \Big\lfloor \frac{s}{2} \Big\rfloor\Big)\mathcal{N}'\left(L-2q, \ell-q, q-s\right), \tag{A.9}$$

with the constraint that when $\ell = q$ one has

$$\mathcal{N}'(L,q,q) = B\Big(\Big\lfloor \frac{L-q}{2} \Big\rfloor, \Big\lfloor \frac{q}{2} \Big\rfloor\Big). \tag{A.10}$$

This is obtained by observing that if $\ell = q$ only 1-strings are allowed and (A.2) gives $\mathcal{N}_n(L,\mathcal{S}) = \lfloor (L-q)/2 \rfloor$.
It is straightforward to check that for even q the ansatz

$$\mathcal{N}'(L,\ell,q) = \frac{q}{\ell} B\Big(\frac{L-\ell}{2}, \frac{q}{2}\Big) B\Big(\frac{\ell}{2}, \frac{q}{2}\Big), \tag{A.11}$$

satisfies (A.9). For odd q the solution of (A.9) is

$$\mathcal{N}'(L,\ell,q) = \frac{\ell-q+1}{\ell} B\Big(\frac{L-\ell}{2}, \frac{q-1}{2}\Big) B\Big(\frac{\ell}{2}, \frac{q-1}{2}\Big). \tag{A.12}$$

The number of eigenstates in the sector with ℓ particles with nonzero Néel overlap $Z'_{Neel}(L,\ell)$ are obtained by summing over all possible values of q as

$$Z'_{Neel}(L,\ell) = \sum_{q=1}^{\ell} \mathcal{N}'(L,\ell,q). \tag{A.13}$$

It is convenient to split the summation in (A.13) considering odd values of q and even q separately. For odd q one obtains

$$\sum_{k=0}^{\ell/2-1} \mathcal{N}'(L,\ell,2k+1) = B\Big(\frac{L}{2} - 1, \frac{\ell}{2} - 1\Big), \tag{A.14}$$

while for even q one has

$$\sum_{k=0}^{\ell/2} \mathcal{N}'(L,\ell,2k) = B\Big(\frac{L}{2} - 1, \frac{\ell}{2}\Big). \tag{A.15}$$

Putting everything together one obtains

$$Z'_{Neel}(L,\ell) = B\Big(\frac{L}{2}-1,\frac{\ell}{2}-1\Big) + B\Big(\frac{L}{2}-1,\frac{\ell}{2}\Big). \tag{A.16}$$

The total number of eigenstates with nonzero Néel overlap $Z_{Neel}(L)$ (cf. (A.1)) is obtained from (A.16) by summing over the allowed values of $\ell = 2k$ with $k = 0,1,\ldots,\ell/2$.

Note that the total number Z_{MG} of parity-invariant eigenstates having non zero overlap with the Majumdar-Ghosh state is obtained from Eq (A.16) replacing $\ell = L/2$, to obtain

$$Z_{MG} = B\Big(\frac{L}{2}-1,\frac{L}{4}-1\Big) + B\Big(\frac{L}{2}-1,\frac{L}{4}\Big). \tag{A.17}$$

Physically, this is due to the fact that the Majumdar-Ghosh state is invariant under $SU(2)$ rotations, which implies that only eigenstates with zero total spin $S = 0$ can have non zero overlap.

Appendix B. Excluding the zero-momentum strings

Here we demonstrate that the total number of eigenstates with nonzero Néel overlap, which do not contain zero-momentum strings, $\widetilde{Z}_{Neel}(L)$ is given as

$$\widetilde{Z}_{Neel}(L) = B\Big(\frac{L}{2},\frac{L}{4}\Big). \tag{B.1}$$

Given a generic M-particle eigenstate of the XXX chain, due to parity invariance, if one excludes the zero-momentum strings only n-strings with length $n \leq M/2$ are allowed. Similarly, the string content is of the form $\widetilde{\mathcal{S}} \equiv \{\tilde{s}_1,\ldots,\tilde{s}_{M/2}\}$, i.e., $\tilde{s}_m = 0\ \forall m > M/2$. Note that due to parity invariance and to the exclusion of the zero-momentum strings one has that $\tilde{s}_m$ is always an even integer. Clearly one has $\sum_{m=1}^{M/2} m\tilde{s}_m = M$.

The total number of parity-invariant quantum numbers $\widetilde{\mathcal{N}}_n$ in the n-string sector is given as

$$\widetilde{\mathcal{N}}_n(L,\widetilde{\mathcal{S}}) = \frac{L}{2} - \frac{1}{2}\sum_{m=1}^{M/2} t_{nm}\tilde{s}_m. \tag{B.2}$$

The proof now proceeds as in Appendix A. One can define the total number of eigenstates with nonzero Néel overla in the sector with ℓ particles and q different strings as $\widetilde{\mathcal{N}}'(L,\ell,q)$. Note that due to parity invariance and the exclusion of zero-momentum strings, q must be even. It is straigtforward to show that $\widetilde{\mathcal{N}}'(L,\ell,q)$ obeys the recursive relation

$$\widetilde{\mathcal{N}}'(L,\ell,q) = \sum_{s=0}^{q/2-1} B\Big(\frac{L}{2}-q+s,s\Big)\widetilde{\mathcal{N}}'\Big(L-2q,\frac{\ell-q}{2},\frac{q}{2}-s\Big), \tag{B.3}$$

with the constraint

$$\widetilde{\mathcal{N}}'(L,1,1) = \frac{L}{2}-1. \tag{B.4}$$

It is straightforward to check that the solution of (B.3) is given as

$$\widetilde{\mathcal{N}}'(L,\ell,q) = \frac{L-2\ell+2}{L-\ell+2} B\Big(\frac{L-\ell}{2}+1, q\Big) B\Big(\frac{\ell}{2}-1, \frac{q}{2}-1\Big). \tag{B.5}$$

After summing over the allowed values of $q = 2k$ with $k = 1, 2, \ldots, \ell/2$ one obtains the total number of eigenstaets with nonzero Néel overlap at fixed number of particles ℓ $\widetilde{Z}'_{Neel}(L,\ell)$ as

$$\widetilde{Z}'_{Neel}(L,\ell) = B\Big(\frac{L}{2}, \frac{\ell}{2}\Big) - B\Big(\frac{L}{2}, \frac{\ell}{2}-1\Big). \tag{B.6}$$

Summing over ℓ one obtains (53). Similar to (A.17) the total number of eigenstates $\widetilde{Z}_{MG}$ with no zero-momentum strings having non-zero overlap with the Majumdar-Ghosh state is obtained from (B.6) replacing $\ell \to L/2$, to obtain

$$\widetilde{Z}_{MG} = B\Big(\frac{L}{2}, \frac{L}{4}\Big) - B\Big(\frac{L}{2}, \frac{L}{4}-1\Big). \tag{B.7}$$

Interestingly, using (A.17) and (B.7), one obtains that the ratio $\widetilde{Z}_{MG}/Z_{MG}$ is given as

$$\frac{\widetilde{Z}_{MG}}{Z_{MG}} = \frac{4}{4+L}. \tag{B.8}$$

Appendix C. Exact Néel and Majumdar-Ghosh overlaps for a small Heisenberg chain

In this section we provide exact diagonalization results for the overlap of both the Néel state and the Majumdar-Ghosh (MG) state with all the eigenstates of the Heisenberg spin chain with $L = 12$ sites. We also provide the corresponding results obtained using the string hypothesis and the overlap formulas (24) and (34), restricting ourselves to eigenstates with no zero-momentum strings.

Appendix C.1. Néel overlap

The overlaps between all the eigenstates of the Heisenberg spin chain and the Néel state are reported in Table C1. The first column in the Table shows the string content $\mathcal{S} \equiv \{s_1, \ldots, s_M\}$, with M being the number of finite rapidities. The number of infinite rapidities $N_\infty = L/2 - M$ is also reported. Note that eigenstates containing infinite rapidities correspond to different S_z eigenvalue. The second column shows $2I_n^+$, with I_n the Bethe-Gaudin-Takahashi quantum number identifying the BGT rapidity of the n-string. Due to the parity invariance only the positive quantum numbers are reported. The total number of independent strings, i.e., $q \equiv \sum_j s_j$, is reported in the third column. The fourth column is the eigenstate's energy eigenvalue E. The last two columns show the squared Néel overlaps and the corresponding result obtained using the Bethe-Gaudin-Takahashi equations, respectively. In the last column only the case with no zero-momentum strings is considered. The deviations from the exact diagonalization results (digits with different colors) have to be attributed to the string hypothesis. Notice that the overlap between the Néel state and the $S_z = 0$ eigenstate in the sector

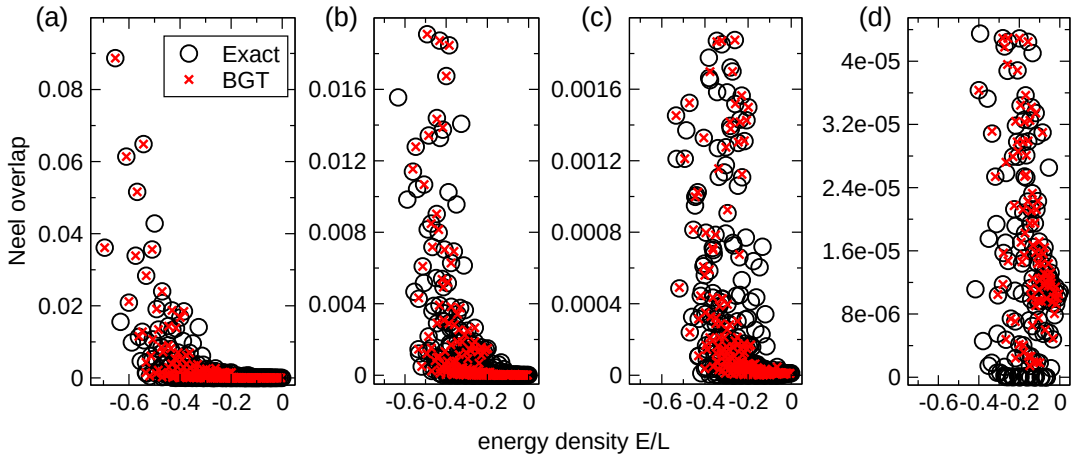

Figure C1. The squared overlap $|\langle N|\lambda\rangle|^2$ between the the Neel state $|N\rangle$ and the eigenstates $|\lambda\rangle$ of the XXX chain with $L = 20$ sites. Only non-zero overlaps are shown. In all the panels the x-axis shows the eigenstate energy density E/L. The circles are the exact diagonalization results for all the non-zero overlaps. The crosses are the Bethe ansatz results obtained using the Bethe-Gaudin-Takahashi equations. The missing crosses correspond to eigenstates containing zero-momentum strings. (a) Overview of all the non-zero overlaps. (b)(c)(d) The same overlaps as in (a) zooming in the regions $[0, 0.2]$, $[0, 0.020]$, and $[0, 4 \cdot 10^{-5}]$. The discrepancies between the ED and the Bethe ansatz results are attributed to the string deviations.

with maximal total spin $S = L/2$ (first column in Table C1), is given analytically as $2/B(L, L/2)$, with $B(x, y)$ the Newton binomial.

Figure C1 plots the squared overlaps $|\langle\lambda|N\rangle|^2$ between the Néel state and the eigenstates of the chain. The overlaps are plotted against the eigenstate energy density $E/L \in [-\log(2), 0]$. The circles are exact diagonalization results for all the chain eigenstates (382 eigenstates), whereas the crosses denote the overlaps calculated using formula (24), and the Bethe-Gaudin-Takahashi equations. Note that only the eigenstates with no zero-momentum strings are shown (252 eigenstates) in the Figure. Panel (a) in the Figure is an overview of all the results. Panels (b)-(d) correspond to zooming to the smaller overlap values $|\langle N|\lambda\rangle| \lesssim 0.02$, $|\langle N|\lambda\rangle| \lesssim 0.002$, and $|\langle N|\lambda\rangle| \lesssim 10^{-5}$.

Clearly, the overlaps decay rapidly upon increasing the energy density. This is expected since the XXX Hamiltonian expectation value over the Néel state is $\langle N|H|N\rangle = -1/2$. Importantly, the agreement between the exact diagonalization results and the results obtained using the BGT equations (**??**) is excellent, confirming the validity of the string hypothesis.

Appendix C.2. Majumdar-Ghosh overlap

The overlap between the Heisenberg chain eigenstates with the Majumdar-Ghosh state are shown in Table C2. The conventions on the representation of the eigenstates is the same as in Table C1. Note that in contrast with the Néel state, only the eigenstates with zero total spin $S = 0$ have non zero overlap, i.e., no eigenstates with infinite rapidities

Bethe states with nonzero Néel overlap ($L = 12$)

String content	$2I_n^+$	q	E	$\|\langle\lambda\|N\rangle\|^2$ (exact)	$\|\langle\lambda\|N\rangle\|^2$ (BGT)
6 inf	-	-	0	0.002164502165	0.002164502165
{2,0} 4 inf	1_1	2	−3.918985947229	0.096183409244	0.096183409244
	3_1		−3.309721467891	0.011288497947	0.011288497947
	5_1		−2.284629676547	0.004542580506	0.004542580506
	7_1		−1.169169973996	0.002752622983	0.002752622983
	9_1		−0.317492934338	0.002116006203	0.002116006203
{4,0,0,0} 2 inf	1_13_1	4	−7.070529325964	0.310133033838	0.310133033838
	1_15_1		−5.847128730477	0.129277023687	0.129277023687
	1_17_1		−4.570746557876	0.085992436024	0.085992436024
	3_15_1		−5.153853093221	0.015256395523	0.015256395523
	3_17_1		−3.916336243695	0.010091113504	0.010091113504
	5_17_1		−2.817696043731	0.004059780228	0.004059780228
{0,2,0,0} 2 inf	1_2	2	−1.905667167442	0.001207238321	0.001207245406
	3_2		−1.368837200825	0.002340453815	0.002325724713
	5_2		−0.681173793635	0.001921010489	0.001939001396
{1,0,1,0} 2 inf	0_10_3	2	−2.668031843135	0.034959609810	-
{6,0,0,0,0,0} 0 inf	$1_13_15_1$	6	−8.387390917445	0.153412152966	0.153412152966
{2,2,0,0,0,0} 0 inf	1_11_2	4	−5.401838225870	0.040162686361	0.041042488913
	3_11_2		−4.613929948329	0.004636541934	0.004730512604
	5_11_2		−3.147465758841	0.001335522556	0.001337334035
{3,0,1,0,0,0} 0 inf	$0_12_10_3$	4	−6.340207488736	0.052743525774	-
	$0_14_10_3$		−5.203653009936	0.015022005621	-
	$0_16_10_3$		−3.788693957250	0.011144489334	-
{1,0,0,0,1,0} 0 inf	0_10_5	2	−2.444293750583	0.005887902992	-
{0,0,2,0,0,0} 0 inf	1_3	2	−1.111855930538	0.001342476001	0.001384980817
{0,1,0,1,0,0} 0 inf	0_20_4	2	−1.560671012472	0.000026982174	-

Table C1. All Bethe states for $L = 12$ having nonzero overlap with the zero-momentum Néel state. The first column shows the string content of the Bethe states, including the number of infinite rapidities. The second and third column show $2I_n^+$, with I_n^+ the BGT quantum numbers identifying the different states, and the number q of independent strings. In the second column only the positive BGT numbers are shown. The fourth column is the Bethe state eigenenergy. Finally, the last two columns show the exact overlap with the Néel state and the approximate result obatained using the BGT equations. In the last column Bethe states containing zero-momentum strings are excluded. Deviations from the exact result (digits with different colors) are attributed to the string hypothesis.

are present, which reflect that the Majumdar-Ghosh state is unvariant under $SU(2)$ rotations.

[1] P. Calabrese and P. Le Doussal, J. Stat. Mech. (2014) P05004.

[2] V. Alba, arXiv:1507.06994.

[3] H. Bethe, Zur Theorie der Metalle. I. Eigenwerte und Eigenfunktionen der linearen Atomkette, Z. Phys. **71**, 205 (1931).

[4] M. Takahashi, *Thermodynamics of one-dimensional solvable models*, Cambridge University Press, Cambridge, 1999.

[5] V. E. Korepin, N. M. Bogoliubov, and A. G. Izergin, *Quantum Inverse Scattering Methods and Correlation Functions*, Cambridge University Press, Cambridge, 1997.

[6] M. Brockmann, J. De Nardis, B. Wouters, and J.-S. Caux, J. Phys. A: Math. Theor. **47**, 345003 (2014).

Bethe states with nonzero Néel overlap ($L = 12$)

String content	$2I_n^+$	q	E	$\lvert\langle\lambda\rvert MG\rangle\rvert^2$ (exact)	$\lvert\langle\lambda\rvert MG\rangle\rvert^2$ (BGT)
{6,0,0,0,0,0}	$1_1 3_1 5_1$	6	−8.387390917445	0.716615769224	0.716615769224
{2,2,0,0,0,0}	$1_1 1_2$	4	−5.401838225870	0.055624700196	0.054033366543
	$3_1 1_2$		−4.613929948329	0.005687428810	0.005582983043
	$5_1 1_2$		−3.147465758841	0.002107475934	0.002107086933
{3,0,1,0,0,0}	$0_1 2_1 0_3$	4	−6.340207488736	0.205891158647	-
	$0_1 4_1 0_3$		−5.203653009936	0.038832154450	-
	$0_1 6_1 0_3$		−3.788693957250	0.006019410923	-
{1,0,0,0,1,0}	$0_1 0_5$	2	−2.444293750583	0.000129601311	-
{0,0,2,0,0,0}	1_3	2	−1.111855930538	0.000011727787	0.000012785580
{0,1,0,1,0,0}	$0_2 0_4$	2	−1.560671012472	0.000330572718	-

Table C2. All Bethe states for $L = 12$ having nonzero overlap with the zero-momentum Majumdar-Ghosh (MG) state. The first column shows the string content of the Bethe states. The second and third column show $2I_n^+$, with I_n^+ the BGT quantum numbers identifying the different states, and the number q of independent strings. In the second column only the positive BGT numbers are shown. Note that, in contrast to Table C1 no states with infinite rapidities are present. The fourth column is the Bethe state eigenenergy. Finally, the last two columns show the exact overlap with the MG state and the approximate result obatained using the BGT equations. In the last column Bethe states containing zero-momentum strings are excluded. Deviations from the exact result (digits with different colors) are attributed to the string hypothesis.

[7] B. Pozsgay, J. Stat. Mech. (2014) P06011.
[8] P. Calabrese and J.-S. Caux, Phys. Rev. Lett. **98**, 150403 (2007).
[9] P. Calabrese and J.-S. Caux, J. Stat. Mech. P08032 (2007).
[10] J. De Nardis, B. Wouters, M. Brockmann, and J.-S. Caux, Phys. Rev. A **89**, 033601 (2014).
[11] B. Pozsgay, M. Mestyán, M. A. Werner, M. Kormos, G. Zaránd, and G. Takács, Phys. Rev. Lett. **113**, 117203 (2014).
[12] B. Wouters, M. Brockmann, J. De Nardis, D. Fioretto, M. Rigol, and J.-S. Caux, Phys. Rev. Lett. **113**, 117202 (2014).
[13] M Mestyán, B. Pozsgay, G. Takács, and M. A. Werner, J. Stat. Mech. (2015) P04001.
[14] E. Ilieveski, J. De Nardis, B. Wouters, J.-S. Caux, F. H. Essler, and T. Prosen, arXiv:1507.02993.
[15] M. Brockmann, B. Wouters, D. Fioretto, J. De Nardis, R. Vlijm, and J.-S. Caux, J. Stat. Mech. (2014) P12009.